TPD study of the adsorption and reaction of nitromethane and methyl nitrite on ordered Pt–Sn surface alloys

ARTICLE *in* SURFACE SCIENCE · AUGUST 1998

Impact Factor: 1.93 · DOI: 10.1016/S0039-6028(98)00198-8

4 AUTHORS, INCLUDING:

David Beck
Oxford Instruments
15 PUBLICATIONS **201** CITATIONS
SEE PROFILE

Bruce Koel
Princeton University
296 PUBLICATIONS **9,075** CITATIONS
SEE PROFILE

ELSEVIER

Surface Science 410 (1998) 170–188

surface science

TPD study of the adsorption and reaction of nitromethane and methyl nitrite on ordered Pt–Sn surface alloys

J.W. Peck, D.I. Mahon, D.E. Beck, B.E. Koel *

Department of Chemistry, University of Southern California, Los Angeles, CA 90089-0482, USA

Received 1 July 1997; accepted for publication 23 February 1998

Abstract

The adsorption and reaction of the isomers nitromethane (CH_3NO_2) and methyl nitrite (CH_3ONO) on two ordered Sn/Pt(111) surface alloys were studied using TPD, AES, and LEED. Even though the Sn–O bond is stronger than the Pt–O bond and Sn is more easily oxidized than Pt, alloying with Sn reduces the reactivity of the Pt(111) surface for both of these oxygen-containing molecules. This is because of kinetic limitations due to a weaker chemisorption bond and an increased activation energy for dissociation for these molecules on the alloys compared to Pt(111). Nitromethane only weakly adsorbs on the Sn/Pt(111) surface alloys, shows no thermal reaction during TPD, and undergoes completely reversible adsorption under UHV conditions. Methyl nitrite is a much more reactive molecule due to the weak CH_3O–NO bond, and most of the chemisorbed methyl nitrite decomposes below 240 K on the alloy surfaces to produce NO and a methoxy species. Surface methoxy is a stable intermediate until ~300 K on the alloys, and then it dehydrogenates to evolve gas phase formaldehyde with high selectivity against complete dehydrogenation to form CO on both alloy surfaces.

Keywords: Alloys; Auger electron spectroscopy (AES); Chemisorption; Low energy electron diffraction (LEED); Low index single crystal surfaces; Methylnitrite; Nitromethane; Platinum; Thermal desorption spectroscopy; Tin

1. Introduction

Reactions at surfaces and interfaces of molecules containing bonds between nitrogen and oxygen are of interest for a wide range of applications, from heterogeneous catalysis [1] to energetic materials [2–4]. Molecules containing the NO_2 functional group are typically quite reactive, and nitroalkanes provide opportunities to study C–N and N–O bond activation on surfaces. Nitromethane (CH_3NO_2), the first member in a homologous series of nitroalkanes, has been investigated previously on several transition metal surfaces, including Ni(111) [5], Pt(111) [6,7], Rh(111) [6], and Au(111) [8], but no other nitroalkanes have been studied in detail. In related work, nitrobenzene ($C_6H_5NO_2$) adsorption on Cu(110) [9] and Au(111) [10,11] has been explored.

Benziger's [5] early study of nitromethane adsorption and reaction on Ni(111) showed that nitromethane decomposed completely on Ni(111) to produce HCN, H_2, adsorbed oxygen, and no NO. Oxygen-predosed Ni(111) was mostly inert to these reactions. Benziger proposed that nitromethane adsorbs through the nitro group, weakening the N–O bonds so that they are more easily

* Corresponding author. Fax: +1 213 740 3972; e-mail: koel@chem1.usc.edu

0039-6028/98/$19.00
PII: S0039-6028(98)00198-8

broken than the C–N bond, even though the C–N bond is the weakest in gas phase nitromethane [12]. Hwang [6] reported that nitromethane adsorbed on the Pt(111) and Rh(111) surfaces decomposed completely. On Rh(111), the decomposition of nitromethane proceeds through dissociation of N–O and C–N bonds to yield CO, H_2, N_2 and CO_2 in TPD. On Pt(111), dissociation of both C–H and N–O bonds left adsorbed CN, which desorbed as C_2N_2 in 85% yield between 750 and 1200 K in TPD. We recently reinvestigated the chemistry of nitromethane on Pt(111) [7] and found that nitromethane adsorbs weakly (11 kcal mol^{-1}) on the Pt(111) surface and only 25% of the chemisorbed monolayer of nitromethane decomposes during TPD to yield H_2O, HCN, NO and CO as the primary products. The principal decomposition pathway is via cleavage of N–O bonds, mostly leaving the C–N bond intact. HREELS [7] indicates that chemisorbed nitromethane adopts a ''pseudo-bidentate'' bonding geometry with $C_s(yz)$ symmetry in which the two oxygens are coordinated inequivalently to the surface with the molecular axis tilted within the molecular plane. Lastly, nitromethane is weakly adsorbed (10.5 kcal mol^{-1}) on Au(111), and adsorption is completely reversible [8]. HREELS determined that nitromethane is bonded on Au(111) in an upright, strongly tilted geometry, suggesting a monodentate coordination to the surface [8].

In homogeneous reactions, nitromethane can isomerize to methyl nitrite (CH_3ONO) with an activation barrier 13 kcal mol^{-1} lower than direct C–N bond cleavage [13], and methyl nitrite has been proposed as an intermediate in the homogeneous thermal decomposition of nitromethane [12]. Methyl nitrite could also be an important intermediate in the heterogeneous decomposition of nitromethane at solid surfaces, but there is not much data available. There are only two previous reports on the adsorption of methyl nitrite on transition metal surfaces, on Ag(111) [14] and Au(111) [8]. Both the Ag(111) and Au(111) surfaces are inert and showed no thermal reaction of methyl nitrite in TPD studies. Pressley et al. [14], however, showed that decomposition of methyl nitrite adsorbed on Ag(111) could be activated by using electron induced dissociation (EID). They found that the reaction of methyl nitrite on Ag(111) proceeds through preferential cleavage of the O–N bond yielding formaldehyde, water and methane. We have recently carried out investigations of methyl nitrite adsorption and reaction on Pt(111) [15], which will be reported separately. Methyl nitrite is very reactive on Pt(111) surfaces, and we find that complete dissociation occurs at very low temperatures (<140 K) to produce primarily NO, CO, and H_2, along with some small amounts of methanol and formaldehyde.

Here, we report on our studies of the adsorption and reaction of nitromethane and methyl nitrite on two Pt–Sn surface alloys. Our goals were to explore further the interesting chemistry and reactivity of Pt–Sn alloys [16–22] using these reactive molecules, and to further investigate the influence of alloyed Sn on Pt surface chemistry using oxygen-containing organic molecules. Briefly, we find that alloying with Sn reduces the adsorption energy of nitromethane compared to that on Pt(111) and completely deactivates the alloy surfaces for thermal dissociation of nitromethane. Methyl nitrite is a very labile molecule compared to nitromethane, and these alloys adsorb CH_3ONO strongly and carry out facile thermal decomposition of this molecule to form NO, formaldehyde ($H_2C{=}O$) and methanol (CH_3OH) desorption products during TPD. The alloys are not as reactive as Pt(111) in this chemistry, decomposing a smaller fraction of the adsorbed methyl nitrite, and this reduced reactivity of the surface both stabilizes surface bound methoxy and inhibits dissociation of formaldehyde, which leads to increased selectivity for the formaldehyde partial oxidation product.

2. Experimental methods

These experiments were performed in two separate stainless steel UHV chambers that were both equipped with instrumentation for AES, LEED, TPD, and Ar^+ ion sputtering. The system base pressures were both $\approx 5\times10^{-11}$ Torr. AES spectra were recorded using a Perkin-Elmer (15-255G) cylindrical mirror analyzer (CMA). LEED was carried out using a Perkin-Elmer (15-180) LEED optics. A shielded UTI 100C quadrupole mass spectrometer (QMS) was used for TPD. All TPD

measurements were made using the QMS in line-of-sight with the sample surface and using a linear heating rate of ≈ 4 K s^{-1}. In performing TPD, the crystal was positioned ≈ 1 mm from an entry aperture of the QMS to reduce contributions to the spectra from the crystal back and edges [23]. A high transparency (97%; 20 lpi) stainless steel screen was spot welded over the end of the QMS ionizer assembly (biased at -55 V) to reduce damage to adsorbed layers on the crystal from low-energy electrons [24].

The Pt(111) crystal was cooled to 95 K using liquid nitrogen or resistively heated to 1200 K. The temperature was recorded by a chromel–alumel thermocouple spot welded to the side of the crystal. The Pt(111) single crystal was cleaned by a combination of Ar^+ sputtering, annealing in UHV, and oxygen treatments. Ion bombardment of the crystal was carried out using 1 kV Ar^+ (3×10^{-5} Torr Ar) for 5–10 min with the sample at 800 K, and then the crystal was annealed to 1000 K in UHV to reorder the surface. Oxygen treatments at 2×10^{-8} Torr O_2 for 5–10 min with the crystal at 800–1000 K followed by flashing in UHV to 1000 K were used to remove submonolayer coverages of surface carbon.

Preparation of the Pt–Sn surface alloys was achieved by evaporating 1–3 ML of Sn on the clean Pt(111) substrate surface followed by annealing the sample to 1000 K for 10 s. Depending upon the initial Sn dose, the annealed surface exhibited either a $p(2 \times 2)$ or a $(\sqrt{3} \times \sqrt{3})R30^\circ$ LEED pattern [25]. These patterns correspond to the (111) face of a Pt_3Sn alloy and a substitutional alloy of composition Pt_2Sn, respectively, rather than Sn adatoms. Angle-dependent low energy ion scattering spectroscopy (LEISS) measurements using 500–1000 eV Li^+ showed that the Sn atoms are almost coplanar with the Pt, protruding $\approx 0.022 \pm 0.005$ nm above the surface in a monolayer surface alloy [26]. LEED *I–V* calculations [27] and X-ray forward scattering [28] have recently confirmed these results. For simplicity, the $p(2 \times 2)$ and $(\sqrt{3} \times \sqrt{3})R30^\circ$ Sn/Pt(111) surface alloys will be referred to in this paper as the (2×2) and $\sqrt{3}$ alloys, respectively. A schematic diagram of these surfaces is provided in Fig. 1.

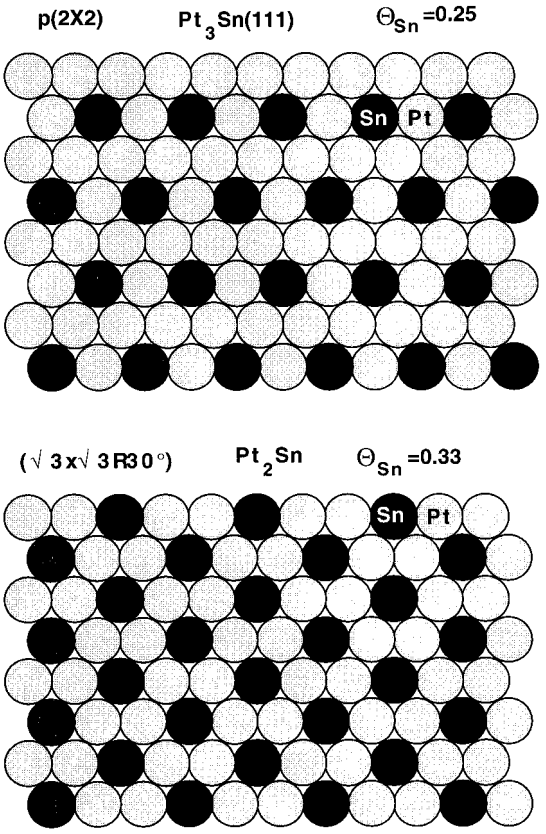

Fig. 1. Schematic drawing of the surface structures for the (2×2) and $\sqrt{3}$ Pt–Sn surface alloys.

Nitromethane (Fisher Scientific, 99%) was degassed by freeze–pump–thaw cycles. Methyl nitrite was prepared from methanol, H_2O, H_2SO_4 and HSO_3ONO according to an accepted procedure [29] and purified by three successive distillations at -25°C under a nitrogen flow through a standard glass distillation column. The sample was further purified to remove gaseous impurities using freeze–pump–thaw cycles. The purity was checked using both IR [30] and in-situ mass spectrometry. Subsequent TPD of methyl nitrite multilayers on Pt(111) did not show the presence of any methanol contaminant (methanol is completely reversibly adsorbed on Pt(111) [22]).

Gas exposures for the TPD studies were made by using a directed beam, multicapillary array doser with the crystal substrate at a temperature below 100 K. Exposures are given in units of

Langmuirs (10^{-6} Torr·s) after the measured values were multiplied by a factor of 115 to account for the doser flux enhancement above the background pressure measured by the ion gauge. This doser correction factor was obtained by comparing uptake curves from exposures produced by the directed beam doser with those from background exposures. The cleanliness and long-range order of all surfaces were checked using AES and LEED prior to each experiment. In addition, the alloy surfaces were checked with LEED following each TPD experiment to ensure that no irreversible adsorbate induced reconstruction occurred.

3. Results

3.1. Adsorption of nitromethane

Nitromethane TPD spectra following nitromethane adsorption on the two Pt–Sn surface alloys are shown in Figs. 2 and 3. The relatively poor signal-to-noise ratio in these spectra is because we chose to utilize the small parent ion (61 amu) rather than, for example, the large 30 amu ion fragment to monitor CH_3NO_2 in order to eliminate ambiguities about the identity of the desorbing species (this also applies to Fig. 4 vide infra). CH_3NO_2 is completely reversibly adsorbed on both surfaces, and desorbs in clearly defined peaks due to the monolayer and multilayer phases. The physisorbed or condensed multilayer peak occurs near 155 K, at the same temperature as that observed on Au(111) [8]. The monolayer desorption temperature is 178 K on the (2×2) alloy and 176 K on the $\sqrt{3}$ alloy, thus it is independent of the Sn concentration in these alloys. A small shift of about 10 K to higher temperatures is seen at the lowest coverages, most clearly on the $\sqrt{3}$ alloy. This indicates attractive lateral interactions within the layer, and this is also consistent with the clustering that causes the population of the multilayer state prior to completion of the monolayer. Importantly, no other gas phase products were detected in TPD. CH_3NO_2 adsorption on the alloys is completely reversible; no thermal decomposition occurs under these conditions.

Alloying Sn into the Pt(111) surface to form these alloys decreases the reactivity of the surface but does not strongly weaken the chemisorption bond energy. The monolayer desorption temperature is 180 K on Pt(111). However, about 25% of the nitromethane monolayer on Pt(111) dissociates during TPD to form two major products, HCN and H_2O, and a small amount of CO and NO [7]. Comparisons of the adsorption kinetics (uptake) curves between Pt(111) and the two Pt–Sn alloys at 100 K reveal that the initial sticking coefficient of nitromethane is the same on all three surfaces. The monolayer saturation coverage of nitromethane is also independent of Sn concentration over this set of three surfaces.

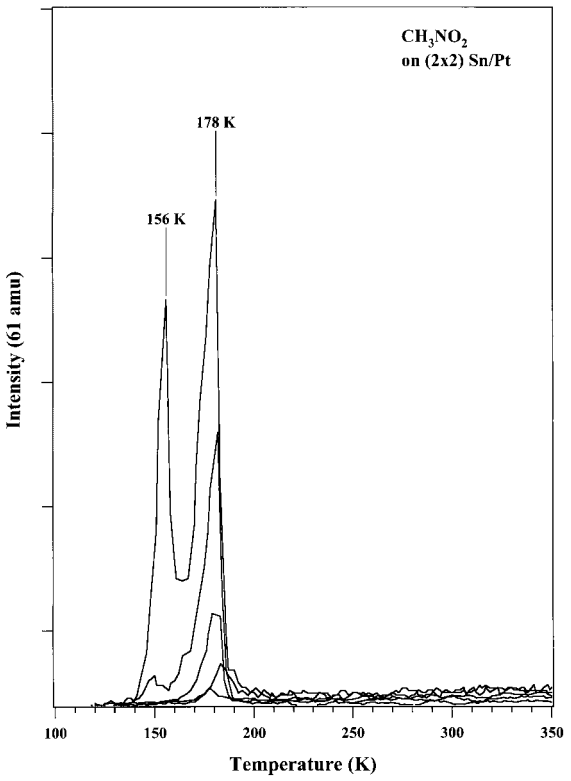

Fig. 2. CH_3NO_2 TPD spectra after CH_3NO_2 exposures on the (2×2) Pt–Sn surface alloy. Exposures used were: 0.05, 0.5, 1.0, 2.5, 5 L.

3.2. Adsorption and reaction of methyl nitrite on the (2×2) Sn/Pt(111) surface alloy

Several TPD spectra obtained for methyl nitrite desorption from the (2×2) alloy are shown in

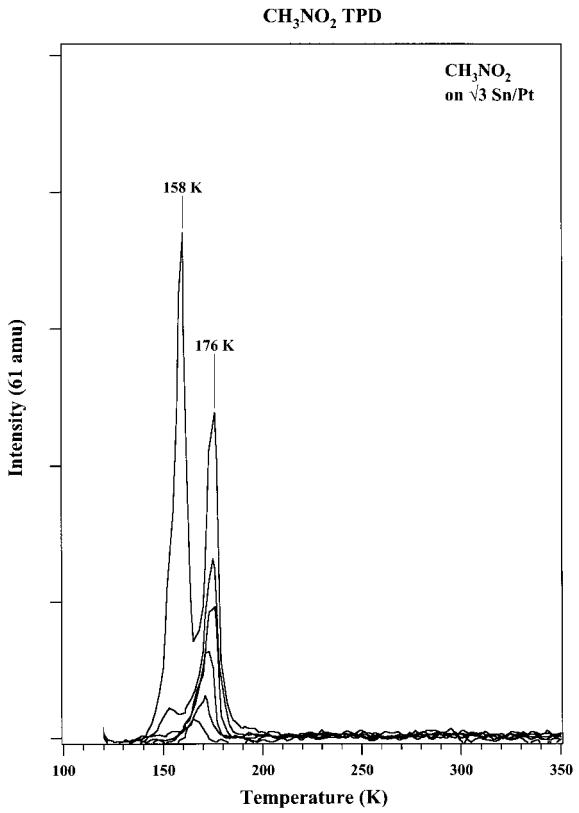

Fig. 3. CH_3NO_2 TPD spectra after CH_3NO_2 exposures on the $\sqrt{3}$ Pt–Sn surface alloy. Exposures used were: 0.05, 0.5, 1.0, 1.5, 2.5, 5 L.

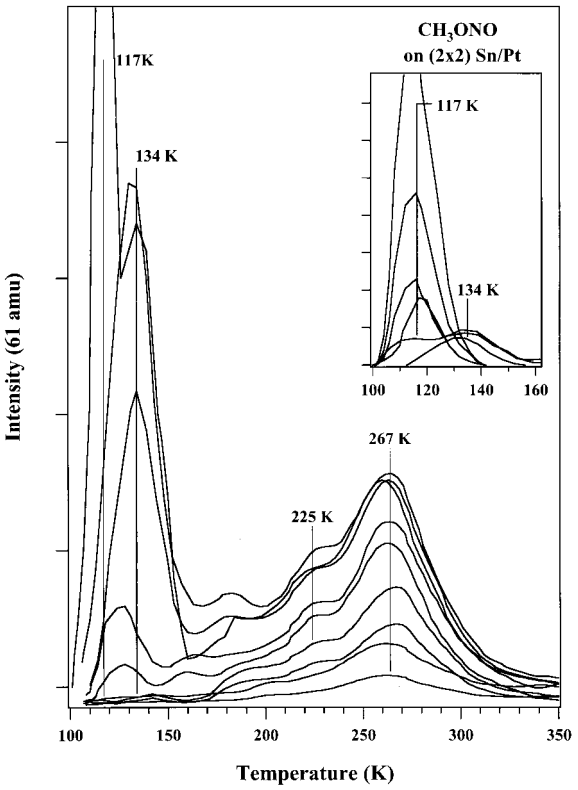

Fig. 4. CH_3ONO TPD spectra after CH_3ONO exposures on the (2×2) Pt–Sn surface alloy. Exposures used were: 0.005, 0.01, 0.10, 0.15, 0.20, 0.25, 0.30, 0.35 L. The inset displays TPD spectra for desorption of multilayers of CH_3ONO obtained at larger doses. Exposures used were: 0.30, 0.35, 0.50, 0.70, 1.2, 2.5, 5 L.

Fig. 4. At low exposures (<0.15 L), methyl nitrite desorbs in two peaks at 225 and 267 K. These TPD peaks are associated with desorption of two chemisorbed states of methyl nitrite. Increasing the exposure to 0.2 L causes a peak at 134 K, which is assigned to desorption of a second physisorbed layer of methyl nitrite adsorbed on top of the monolayer. At higher coverages produced by doses larger than 0.4 L, as shown in the inset to Fig. 4, a peak is observed at 117 K that is assigned to desorption of multilayers of physisorbed methyl nitrite. This multilayer desorption peak agrees well with a peak also observed at 117 K by Pressley et al. [14] in their TPD study of methyl nitrite adsorbed on Ag(111), which they assigned to methyl nitrite desorption from the multilayer.

Signals at 32, 31, 30 and 29 amu were observed during TPD to watch for possible gas phase products arising from cleavage of the O–NO bond, including methanol, NO and formaldehyde, and to determine the cracking fractions produced at these masses from methyl nitrite desorption. Mass 46 was monitored to detect a possible NO_2 product. Signals at 58, 56, 54, 44, 43, 28, 27, 18, 17, 16, 12 and 2 amu were also observed to measure the sample purity and possible dehydrogenation and decomposition products. Only those signals that indicated detection of a significant gas-phase desorption product are discussed here.

Fig. 5 shows TPD spectra of the significant products detected following dosing a monolayer of methyl nitrite, at an exposure of 0.3 L, on the (2×2) alloy. The desorption peaks at 134 K are

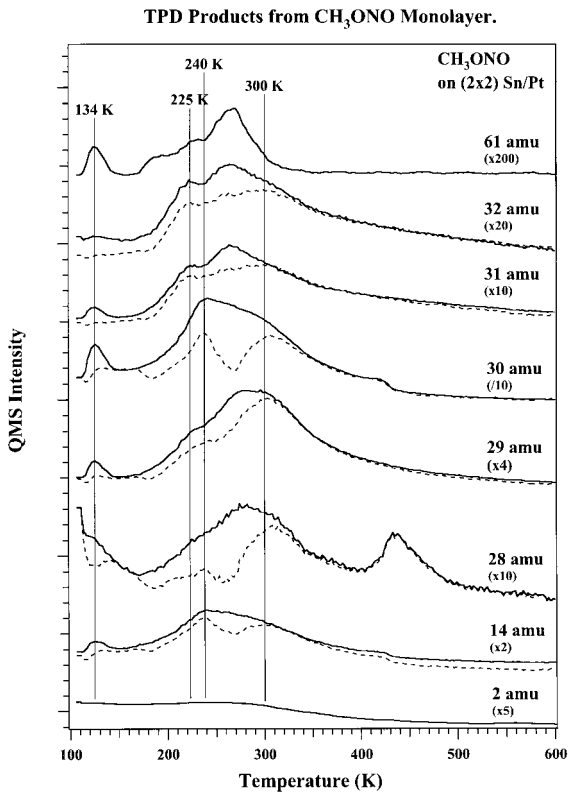

Fig. 5. TPD spectra of products from the reaction of CH_3ONO on the (2×2) Pt–Sn surface alloy. CH_3ONO was dosed on the alloy at 108 K to a coverage exceeding one monolayer. The dashed lines denote better estimates for the desorption of products after removal of CH_3ONO cracking contributions based on CH_3ONO multilayer spectra.

all cracking fractions associated with desorption of the second physisorbed layer of methyl nitrite. The mass fragment ion intensities in this peak have relative intensities of: $30>29>14\gg32\gg61$. The ion intensities observed in this experiment are in agreement with the previous TPD studies carried out by Pressley et al. [14] and with work done by Irion et al. [31] using Fourier Transform Mass Spectrometry (FTMS). The dashed curves in Fig. 5. were constructed by subtracting the appropriately scaled methyl nitrite cracking contributions from the measured TPD spectra to reveal the non-cracking contributions to the curves. The dashed curves show more clearly new desorption peaks at 225, 240, and 300 K. These peaks have intensity variations that cannot be attributed simply to desorption of a single product. We interpret these results to indicate desorption of three separate products from the dissociation of methyl nitrite on the (2×2) surface alloy: NO, CH_3OH, and CH_2O.

The nascent products from the decomposition of CH_3ONO in the monolayer are NO, which desorbs in a peak (30 and 14 amu) at 240 K (the peak at 300 K is likely a cracking fraction of formaldehyde, vide infra), and a surface methoxy intermediate. Two independent products that arise from the subsequent thermal reaction of methoxy are observed during TPD experiments in peaks at 225 and 300 K. The intensities and overlap of the TPD peaks at 30 amu for these products make deconvolution of the 30 amu spectra difficult, but the NO desorption peak at 240 K can be identified by observing its corresponding ion fragment at 14 amu. Identifying and deconvoluting the contributions of other desorption products proved to be more of a challenge. The key to assigning the products was to look at the ordering of the relative ion intensities and to compare those to known reference cracking patterns. For the 225 K peak, the relative intensity pattern was $31>32>29$ amu, and this corresponded well with the methanol reference mass spectrum [22]. Conversely, the 300 K peak had relative ion intensities corresponding to $30>29>28>31>32$ amu. This is inconsistent with methanol, and this ion fragment pattern corresponds well to formaldehyde reference mass spectra [32]. There is considerable intensity for the 300 K peak at 31 and 32 amu, which are not channels for formaldehyde cracking. This could be explained by a second higher temperature desorption state of methanol.

Throughout this paper, we will use the signals at 32, 30, and 29 amu in TPD traces to follow the production of CH_3OH, NO, and CH_2O, respectively. For convience, we will label these TPD spectra as due to CH_3OH, NO, and CH_2O desorption, but we emphasize that these spectra do not correspond solely to these products and also contain contributions from one or more other species because of cracking fragments. TPD spectra monitored at 32 (CH_3OH), 30 (NO), and 29 (CH_2O) amu after increasing CH_3ONO exposures on the (2×2) alloy are shown in Fig. 6. The

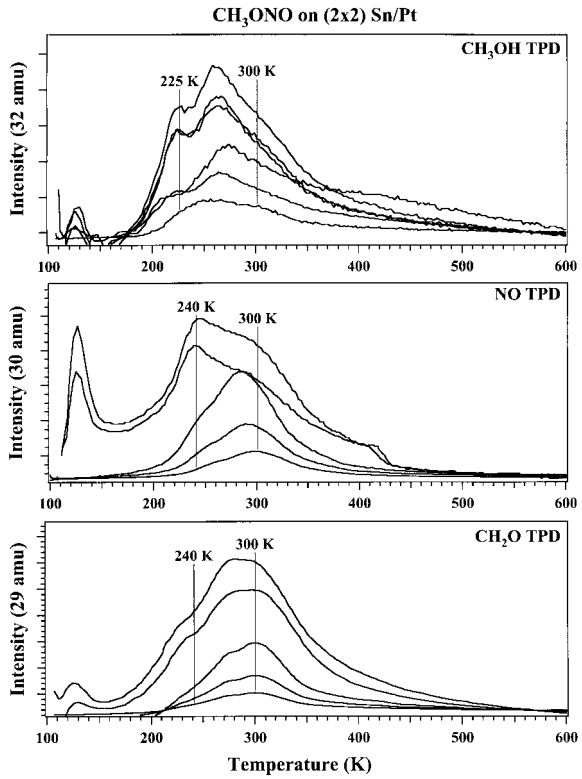

Fig. 6. TPD spectra obtained for 32, 30 and 29 amu signals after CH_3ONO exposures on the (2×2) Pt–Sn surface alloy. These spectra can be used to follow desorption of CH_3OH, NO and $H_2C{=}O$ products, respectively. Exposures used were: 0.005, 0.01, 0.10, 0.20, 0.21, 0.30 L.

30 amu TPD spectra show that a peak initially arises at 300 K, but the spectra broaden to both higher and lower temperatures with increasing coverage, forming a peak at 240 K and a high-temperature shoulder extending to 420 K. The 240 K peak coincides with NO desorption following NO adsorption on the (2×2) alloy [33] and is assigned to desorption rate-limited NO production from the decomposition of CH_3ONO. Desorption signals at higher temperatures are due to cracking fractions of other molecules. The TPD spectra at 29 amu show little coverage dependence, but small features at 225 and 267 K can be observed at higher coverages in the TPD spectra in addition to a peak at 300 K. The peak at 300 K is assigned to formaldehyde desorption, but this desorption temperature is considerably higher than that observed for formaldehyde desorption following formaldehyde adsorption on Pt(111) surface where a desorption temperature of 240 K was observed [32]. Since these alloy surfaces typically reduce the adsorption energy of molecules, [16–22], we assign the formaldehyde evolution at 300 K to desorption that is rate-limited by the dehydrogenation of a methoxy intermediate present on the surface following cleavage of the O–NO bond in adsorbed CH_3ONO. Redhead analysis [34] of the spectra indicates an activation energy of $\sim$16.5 kcal mol^{-1} for this reaction. The peak at 240 K arises from desorption rate-limited formaldehyde evolution and the feature at 267 K arises from methyl nitrite cracking in the ionizer of the QMS (see Fig. 5). The 32 amu TPD spectra show three peaks at 225, 267, and 300 K, but the peak at 267 K arises from methyl nitrite cracking. Both peaks at 225 and 300 K are due to the desorption of methanol formed from the hydrogenation of surface methoxy, and both peaks are reaction rate-limited. Previous studies of the adsorption of methanol on the (2×2) alloy surface [22] showed that methanol desorbs below 190 K. The peak at 225 K is limited by the hydrogenation rate of surface methoxy. Methanol desorption near 300 K is rate-limited by the production of surface hydrogen that occurs when surface methoxy undergoes dehydrogenation to form formaldehyde.

An uptake plot for methyl nitrite adsorption on the alloy surface was constructed from the peak areas measured in TPD and is shown in Fig. 7. As we saw in the TPD figures, but now as more clearly revealed, the amount of CH_3ONO, NO, CH_3OH, and $H_2C{=}O$ desorbing from the alloy surface increased at a steady rate until an exposure of $\approx$0.2 L where all of the peaks saturated. Methyl nitrite desorption at the lowest doses signals partially reversible adsorption even at low coverages. At exposures above 0.2 L, a methyl nitrite peak at 134 K was observed that saturated at an exposure of 0.4 L. Finally, above 0.4 L exposures, a peak at 117 K grew in due to condensation of CH_3ONO multilayers.

The coverages of NO and CH_3ONO corresponding to the desorption peak areas have been calibrated in absolute units of CH_3ONO coverage [15]. This was done by first calibrating the NO

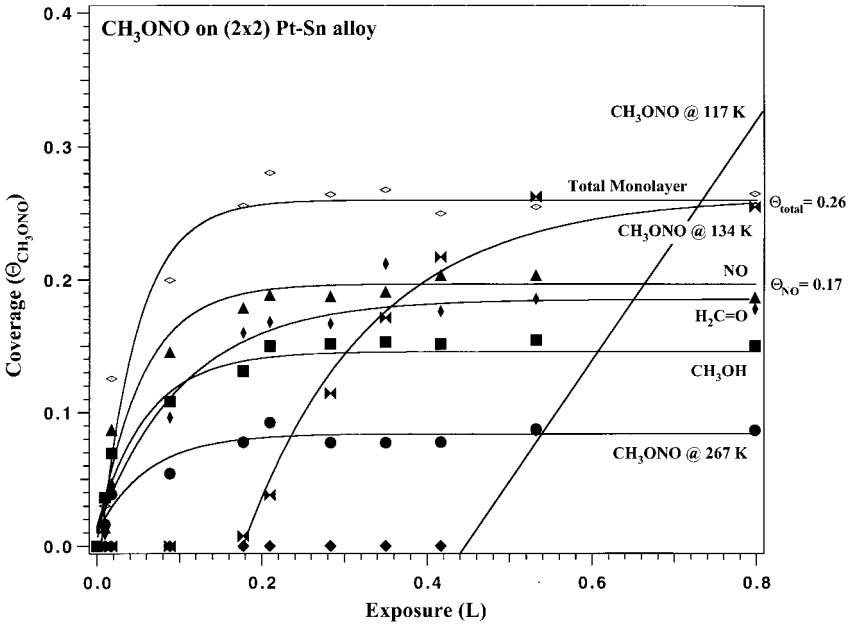

Fig. 7. Uptake curves constructed from TPD peak areas following the adsorption of CH_3ONO on the (2×2) Pt–Sn surface alloy. The amount of NO desorbed from the reaction of CH_3ONO is 0.17 ML, which represents 70% of the total monolayer coverage of 0.26 ML. The CH_2O and CH_3OH yields are not calibrated and are shown in arbitrary units.

desorption areas to the known coverage of NO from NO exposure on Pt(111), and then using a 1-to-1 correspondence of the amount of CH_3ONO decomposition to NO yield. The CH_3ONO area was calibrated to CH_3ONO coverage by forcing the uptake curve on Pt(111) to have a constant slope, i.e. constant sticking coefficient, for the region at low coverage where the NO yield reflects the CH_3ONO coverage since there is no CH_3ONO desorption, and the region at high coverage where CH_3ONO is the only desorbed species. We note that we did not calibrate the CH_2O and CH_3OH curves to CH_3ONO coverage, but they are shown in arbitrary units to correlate with the NO yield from CH_3ONO decomposition. All of the decomposition products are evolved from the surface with a similar coverage dependence. The total monolayer coverage of CH_3ONO is 0.26 ML, as obtained by summing the amount of CH_3ONO that undergoes decomposition (identified by the NO yield; 0.17 ML) with the reversibly adsorbed CH_3ONO (0.09 ML). This is also the saturation coverage obtained for methyl nitrite adsorption on the Pt(111) surface [15]. These results show that Sn does not act as an effective site-blocker to the adsorption of CH_3ONO. We also note that the methyl nitrite monolayer coverage of 0.26 ML is a value close to the reported saturation coverage of methyl nitrite on Ag(111) of 0.3 ML [14].

The methyl nitrite peak at 134 K was observed in previous experiments for methyl nitrite adsorption on Ag(111) [16] and was associated with a weakly chemisorbed state of methyl nitrite adsorbed in the monolayer. The uptake curves produced in this experiment and on the Pt(111) surface [15] show that this state of methyl nitrite desorbing at 134 K has a coverage of $\sim$0.25 ML, equal in coverage to the chemisorbed monolayer, and so on the Pt(111) and Pt–Sn alloy surfaces, this state should be associated with a second, physisorbed layer on top of the monolayer.

3.3. *Adsorption and reaction of methyl nitrite on the $\sqrt{3}$ Sn/Pt(111) surface alloy*

Fig. 8 shows CH_3ONO TPD spectra for increasing coverages of methyl nitrite adsorbed on the

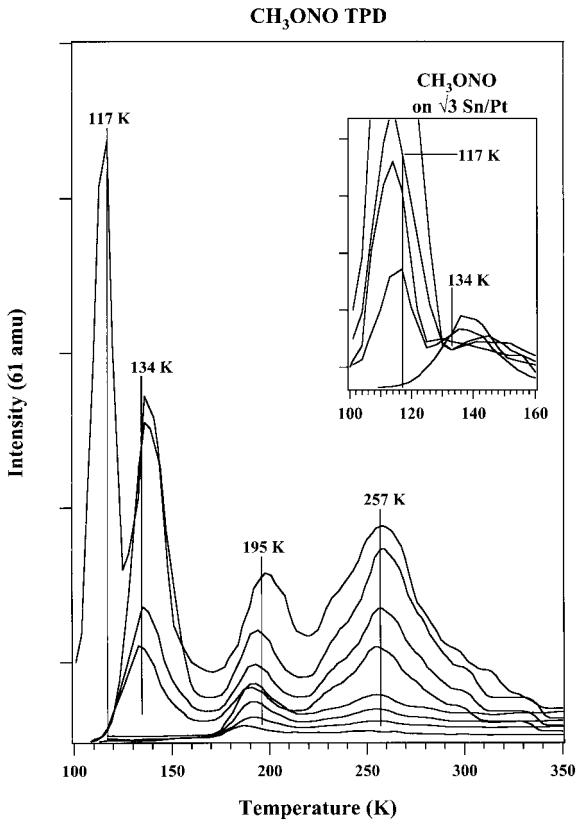

Fig. 8. CH_3ONO TPD spectra after CH_3ONO exposures on the $\sqrt{3}$ Pt–Sn surface alloy. Exposures used were 0.005, 0.01, 0.10, 0.15, 0.20, 0.25, 0.30, 0.35 L. The inset displays TPD spectra for desorption of multilayers of CH_3ONO obtained at larger doses. Exposures used were: 0.35, 0.50, 0.80, 2.5, 5 L.

$\sqrt{3}$ alloy. Two peaks occur at 195 and 257 K at submonolayer coverages (<0.2 L), with the odd observation that the peak at 195 K grows in first. The peak at 257 K is assigned to desorption of a strongly chemisorbed state of methyl nitrite on the $\sqrt{3}$ alloy surface. The origin of the peak at 195 K is still unclear, but we believe it to be desorption of a separate chemisorbed state of methyl nitrite. At slightly higher coverages formed from doses above 0.2 L, a peak at 134 K is observed, and this peak corresponds well with the physisorbed second layer desorption peak seen on both the (2×2) alloy and the clean Pt(111) surface [15]. The peak from multilayer desorption grows in at 117 K after exposures above 0.4 L on the $\sqrt{3}$ alloy, as seen in the inset to Fig. 8, and was not saturated in intensity at exposures of 20 L.

Fig. 9 shows a number of TPD spectra that can be used to determine the desorbed reaction products from a methyl nitrite monolayer (0.4 L) adsorbed on the $\sqrt{3}$ alloy. The fragment ion relative intensities for the multilayer methyl nitrite desorption peak at 117 K agree with those observed for methyl nitrite multilayer TPD on the (2×2) alloy. Subtracting scaled (using the multilayer reference) methyl nitrite contributions from the TPD spectra gives the dashed lines shown in Fig. 9 and helps to identify several product peaks. The 30 and 14 amu spectra show a peak at 217 K that is assigned to desorption of NO. The higher temperature peak at 334 K is attributed to a crack-

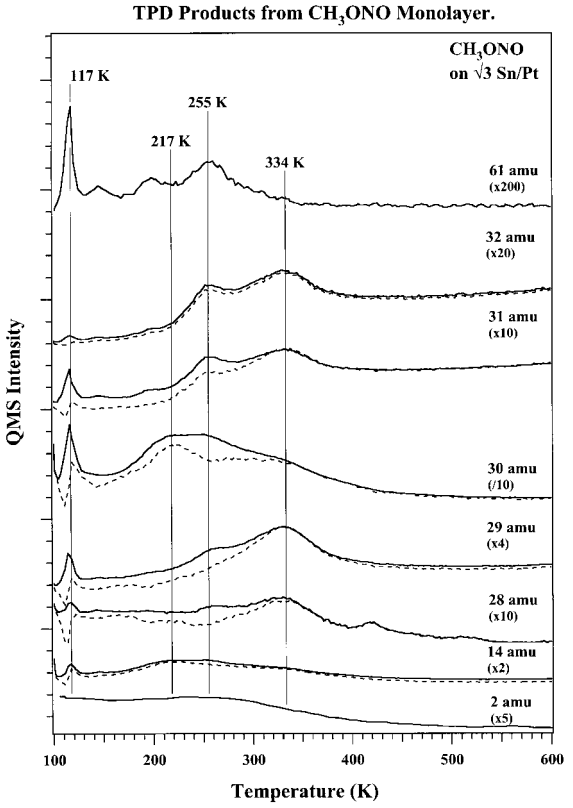

Fig. 9. TPD spectra of products from the reaction of CH_3ONO on the $\sqrt{3}$ Pt–Sn surface alloy. CH_3ONO was dosed on the alloy at 108 K to a coverage exceeding one monolayer. The dashed lines denote better estimates for the desorption of products after removal of CH_3ONO cracking contributions based on CH_3ONO multilayer spectra.

ing fraction from formaldehyde desorption. A peak at 334 K is observed as the primary desorption feature in the 29 amu TPD spectrum. Two features are observed in the TPD spectra at 32 amu, a peak that corresponds in temperature to the chemisorbed methyl nitrite desorption peak at 255 K and a peak coincident in temperature with formaldehyde desorption at 334 K. Subtracting the methyl nitrite contribution from this TPD spectrum indicates that another product is desorbed at 255 K and 334 K, which we assign to reaction rate-limited methanol desorption.

As we found on the (2×2) alloy, the main products from the decomposition of CH_3ONO on the $\sqrt{3}$ alloy are NO, which has a primary desorption peak at 217 K, and methanol and formaldehyde. We believe that a methoxy intermediate is formed at a low temperature, and further reaction of this species yields at least two different gas-phase desorption products, methanol and formaldehyde. The peaks at 255 and 334 K in these TPD spectra follow the same fragment ion intensity ratios as those observed for the two product channels on the (2×2) Sn/Pt surface. The peaks are better separated here than on the (2×2) alloy, and therefore, we have a better opportunity to elucidate the contributions of the two products to the peaks in our TPD spectra.

The high-temperature peak at 334 K in the 29 amu spectra is assigned to formaldehyde desorption from the surface. The intensity of the peaks at 255 and 334 K in the 31 and 32 amu spectra provide evidence for methanol desorption formed from the hydrogenation of methoxy. Just like on the (2×2) alloy, no CO or H_2 is observed as a gas-phase product in TPD, indicating that methoxy does not undergo complete dehydrogenation.

A series of TPD spectra monitoring signals at 32 (CH_3OH), 30 (NO), and 29 (CH_2O) amu are shown in Fig. 10 for increasing CH_3ONO coverages on the $\sqrt{3}$ alloy. The 30 amu spectra show a peak at 217 K at low coverages, and then a broad feature from 200 to 400 K emerges at higher coverages with a peak near 334 K. This latter peak is assigned to a cracking fraction from desorption of formaldehyde, which also generates cracking

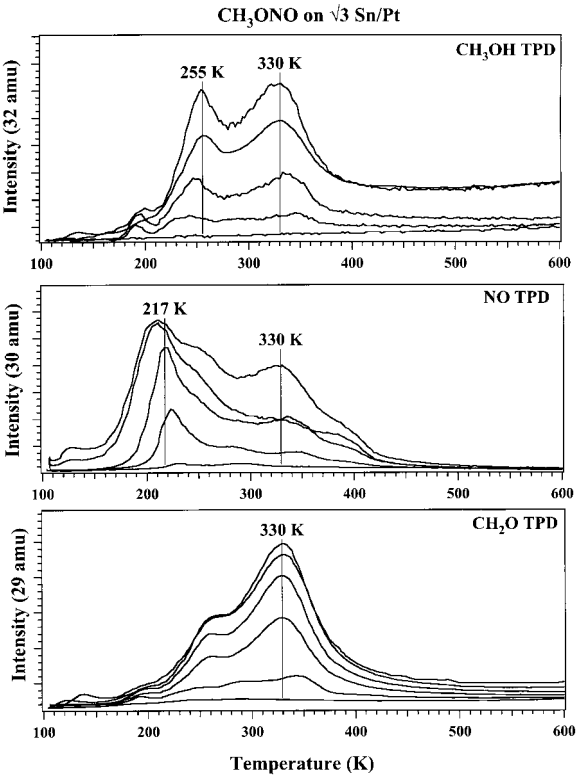

Fig. 10. TPD spectra obtained for 32, 30 and 29 amu signals after CH_3ONO exposures on the $\sqrt{3}$ Pt–Sn surface alloy. These spectra can be used to follow desorption of CH_3OH, NO and $H_2C{=}O$ products, respectively. Exposures used were: 0.005, 0.01, 0.1, 0.15, 0.20, 0.25 L.

fractions at 29 and 28 amu. The peak at 217 K is assigned to NO desorption rate-limited evolution of NO produced from the dissociation of the O–NO bond of methyl nitrite, because this peak agrees well with the NO desorption peak following NO adsorption on the $\sqrt{3}$ alloy [33]. The 29 amu TPD spectra show a primary peak at 330 K due to formaldehyde desorption and a shoulder at 255 K arising from a cracking fraction of methanol desorption (which has its primary peak at 31 amu). Formaldehyde desorption at 330 K is $\approx$100 K higher in temperature than for formaldehyde desorption from a formaldehyde adlayer on Pt(111) [32], and because the addition of Sn generally reduces the activation energy of adsorbed molecules, we assign this peak to a reaction rate-limited evolution of formaldehyde. The TPD

spectra at 32 amu show two peaks at 255 and 330 K. The intensities of these peaks indicate that they are not simply the result of cracking of methyl nitrite or formaldehyde and are assigned to desorption of a methanol product. The temperature of these methanol desorption states is considerably higher than the 165 K observed for methanol desorption after methanol adsorption on the $\sqrt{3}$ Sn/Pt alloy surface [22], and so both peaks are due to reaction rate-limited processes.

Fig. 11 shows an uptake plot for methyl nitrite adsorption on the $\sqrt{3}$ alloy surface constructed from the peak areas measured in TPD. The overall adsorption kinetics, coverages, and branching ratios for reversible and irreversible adsorption is very similar to that for the (2×2) alloy shown in Fig. 7. We note that the saturation monolayer coverage is 0.26 ML, independent of the concentration of Sn on the surface. The $\sqrt{3}$ alloy is less reactive, however, and the NO yields on the alloys show that the irreversibly adsorbed fraction of methyl nitrite changes from 70% on the (2×2) surface alloy to 58% on the $\sqrt{3}$ alloy.

We also used LEED in these investigations. Exposing the surface alloys to monolayer coverages of nitromethane and methyl nitrite, using exposures near saturation, only caused an increase in the diffuse background intensity for both alloy surfaces; chemisorption occurs into a disordered adlayer phase. The $p(2\times2)$ and $(\sqrt{3}\times\sqrt{3})R30^\circ$ LEED patterns were still visible and sharp, indicating that the adsorption of these molecules does not significantly alter the 2D structure of these surface alloys. After TPD, the LEED pattern retained its initial pattern, signifying that the thermal reaction of methyl nitrite does not alter the 2D structure of the substrate.

4. Discussion

4.1. Adsorption of nitromethane (CH_3NO_2) on Pt–Sn surface alloys

Adsorption of CH_3NO_2 on either of the Sn/Pt(111) surface alloys studied here does not

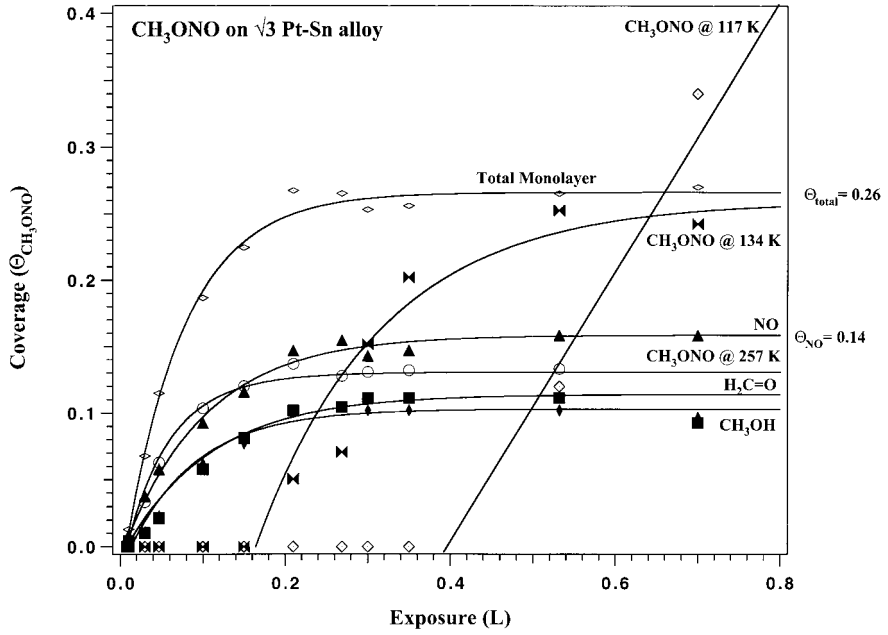

Fig. 11. Uptake curves constructed from TPD peak areas following the adsorption of CH_3ONO on the $\sqrt{3}$ Pt–Sn surface alloy. The amount of NO desorbed from the reaction of CH_3ONO is 0.14 ML which represents 58% of the total monolayer coverage of 0.26 ML. The CH_2O and CH_3OH yields are not calibrated and are shown in arbitrary units.

lead to thermal activation of either the C–N or the N–O bonds of nitromethane upon heating under UHV conditions; the adsorption of nitromethane on these alloys is completely reversible. The desorption temperature of nitromethane from the monolayer decreased from 178 K on the (2×2) alloy to 176 K on the $\sqrt{3}$ alloy. The minimal change in desorption temperature is illustrated in Fig. 12, which also compares the monolayer desorption peak for nitromethane on Pt(111) [7]. On Pt(111), the first 25% of the chemisorbed monolayer decomposes during TPD, and so the thermal desorption of nitromethane takes place from a coadsorbed layer containing dissociation products. However, it seems clear that the presence of Sn in the surface layer of the two Pt–Sn surface alloys hardly affects the bonding interaction between nitromethane and the alloy surfaces compared to Pt(111). If anything, the alloys bond nitromethane slightly more weakly. Redhead analysis provides a rough estimate of the decrease in the adsorption energy from 10.8 kcal mol^{-1} for Pt(111) and (2×2) alloy to 10 kcal mol^{-1} for the $\sqrt{3}$ Sn/Pt alloy. The Sn–O bond is stronger than the Pt–O bond, and Sn is more easily oxidized than Pt, and so it was reasonable to expect that Sn atoms at the surface of the alloy would lead to stronger bonding of nitromethane than on Pt(111). Evidently, the bonding interactions between Pt and Sn in the alloy [35] change the electronic structure of Sn, so that it is less oxophilic than Sn at the surface of bulk Sn, and do not appreciably increase the oxophilicity of Pt compared to that on bulk Pt. Recently, we have observed similar results in studies of methanol, ethanol, and water [22], and ethylene oxide [36], in which these oxygen-containing molecules were also bound less strongly on the Pt–Sn alloys than on Pt(111).

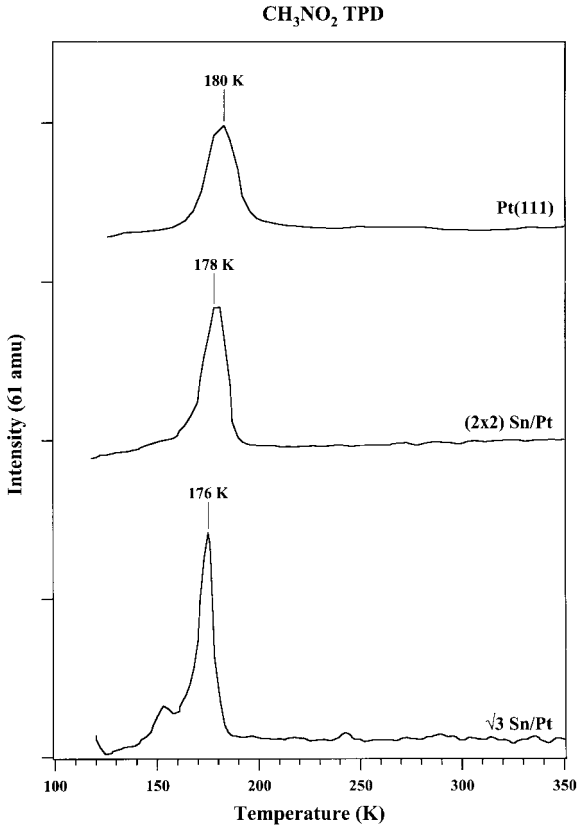

Fig. 12. CH_3NO_2 TPD spectra for near monolayer coverages of CH_3NO_2 on Pt(111) and the (2×2) and $\sqrt{3}$ Pt–Sn surface alloys.

UPS and HREELS of the chemisorbed nitromethane monolayer on Pt(111) [7] show only small changes in the electronic structure and vibrational spectra of nitromethane compared to condensed phase results, consistent with the small adsorption energy of molecular nitromethane. HREELS data indicate that chemisorbed nitromethane adopts a ''pseudo-bidentate'' bonding geometry with $C_s(yz)$ symmetry in which the two oxygens are coordinated inequivalently to the surface with the molecular axis tilted within the molecular plane. We have not yet examined spectroscopically the bonding of nitromethane on these Pt–Sn alloys, but given the nearly identical adsorption energies, it is likely that the bonding is similar to that on Pt(111).

The presence of Sn at the surface of the alloy also acts to suppress the reactivity of adsorbed nitromethane compared to Pt(111). Heating of adsorbed nitromethane during TPD leads primarily to gas phase HCN and H_2O, with a minor amount of NO and CO, as a result of decomposition of about 25% of the adsorbed nitromethane. The principal decomposition pathway on Pt(111) is via cleavage of N–O bonds, mostly leaving the

C–N bond intact. One may have also expected that the influence of surface Sn would be to activate the oxygen bonds in molecules leading to increased thermal decomposition. Based on this work, and also our previous studies of other oxygenates [7,8,15,22], this does not occur under UHV conditions. An increased activation energy for dissociation on the alloys compared to Pt(111) for nitromethane and the other molecules mentioned above causes kinetic limitations on achieving oxidation of the alloy which is preferred thermodynamically. These barriers must arise from bonding interactions between the Pt and Sn to change the surface electronic structure since blocking of reactive ensembles of Pt atoms by Sn should not play a significant role for these oxygenates where Sn is reactive in principle.

These Pt–Sn alloys also do not sufficiently activate isomerization of nitromethane to methyl nitrite for us to observe it. If this isomerization would have occurred to any appreciable extent, we would have observed the decomposition products characteristic of methyl nitrite since, as we have seen, this molecule partially decomposes on the alloy surfaces.

It is of interest to note that nitromethane is much less reactive compared to NO_2, a radical, on both Pt(111) and these Pt–Sn alloys. NO_2 adsorbs on Pt(111) with an adsorption energy of at least 19 kcal mol^{-1} in a bridge-bonded configuration with C_s symmetry, in an upright position through a dative bond to an oxygen atom and a covalent bond to the nitrogen atom [37–39]. About 80% of the chemisorbed NO_2 layer is decomposed upon heating, at temperatures as low as 170 K. Recently, we have also shown that NO_2 is strongly adsorbed on these Pt–Sn alloys, and heating to 150 K leads to extensive oxidation of the alloy surface [40].

4.2. Reactions of methyl nitrite (CH_3ONO) on Pt–Sn surface alloys

The contrast in chemistry between nitromethane and methyl nitrite comes from the difference in N–O bond strengths in these two molecules. The bond dissociation energy of the CH_3O–NO bond is only 42 kcal mol^{-1} [13], which is much weaker than the 78 kcal mol^{-1} N–O bond energy in CH_3NO_2. Cleavage of the N–O bond in methyl nitrite should be more facile, and if this bond is broken, the dissociation should yield NO and a methoxy species on the surface. Our TPD data confirm the more reactive nature of adsorbed methyl nitrite and show significant NO desorption from methyl nitrite decomposition on the Pt–Sn surface alloys. Detection of methanol and formaldehyde as products is consistent with a mechanism in which the dissociation of methyl nitrite proceeds through a methoxy intermediate.

A brief review of our results for methyl nitrite adsorption and reaction on the Pt(111) surface [15] is useful to put the chemistry of methyl nitrite on the Pt–Sn surface alloys into context. Methyl nitrite is irreversibly adsorbed on Pt(111); complete decomposition of the chemisorbed methyl nitrite monolayer occurs during TPD and desorption of NO, CH_3OH, CO and H_2 is observed [15]. Fig. 13 presents a comparison of methyl nitrite TPD spectra, illustrating that the addition of Sn stabilizes adsorbed methyl nitrite against decomposition. New molecular desorption states are observed on the alloys, and there is only a small change in desorption activation energies on the two alloys. The low-temperature peak at 134 K common to all three surfaces arises from a physisorbed state of methyl nitrite present in the second layer. Methyl nitrite is irreversibly adsorbed on Pt(111), and so we cannot estimate the molecular adsorption energy other than that it exceeds the value of the activation energy barrier to decomposition of <11 kcal mol^{-1} [15]. Redhead analysis [34] of the highest temperature peak from the alloys shows a reduction in desorption activation energy from 16.3 kcal mol^{-1} on the (2×2) alloy to 15.6 kcal mol^{-1} on the $\sqrt{3}$ alloy.

On Pt(111), methyl nitrite is molecularly adsorbed at 100 K, but the activation barrier to decomposition is small (<11 kcal mol^{-1}), and methyl nitrite decomposition occurs below 195 K at monolayer coverages. At low concentrations, the methoxy intermediate produced by O–NO bond cleavage completely dissociates below 195 K to form CO and H_2 desorption products. At high initial coverages, coadsorbates poison the surface and stabilize methoxy so that hydrogenation

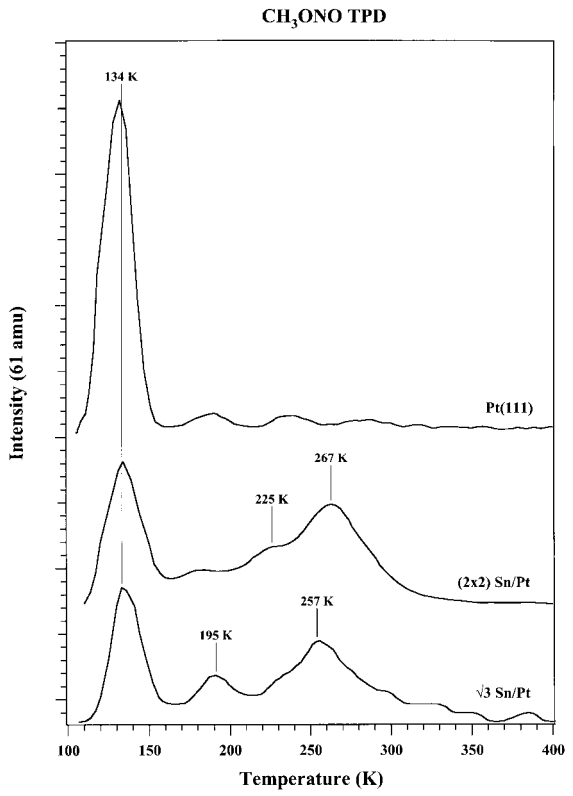

Fig. 13. CH_3ONO TPD spectra for coverages exceeding one monolayer of CH_3ONO on Pt(111) and the (2×2) and $\sqrt{3}$ Pt–Sn surface alloys.

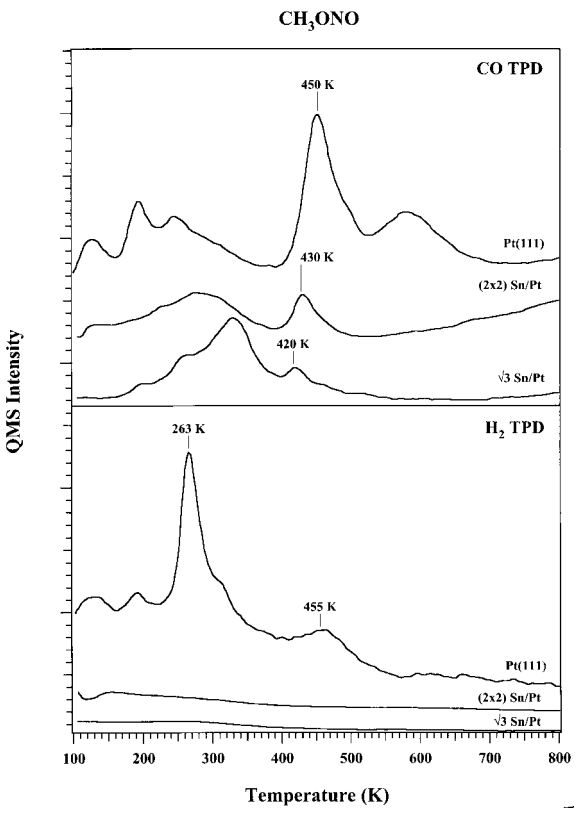

Fig. 14. TPD spectra at 28 and 2 amu after 0.30 L CH_3ONO exposures on Pt(111) and the (2×2) and $\sqrt{3}$ Pt–Sn surfaces. These spectra can be used to follow desorption of CO and H_2, respectively.

occurs to form methanol, which desorbs in a desorption rate-limited peak at 195 K. A small amount of formaldehyde desorption is also observed, although this product accounts for less than 5% of the adsorbed methyl nitrite. HREELS and UPS warm-up experiments for methyl nitrite on Pt(111) show that the molecule is completely dissociated by 165 K, consistent with our TPD data. These results also indicate that at least a portion of the methyl nitrite monolayer is dissociatively adsorbed on the Pt(111) surface at 110 K.

In order to visualize more clearly how alloyed Sn alters the surface reactivity of Pt–Sn alloys compared to Pt(111), Figs. 14–16 compare CO, H_2, NO, CH_3OH, and $H_2C{=}O$ desorption from the reaction of a methyl nitrite monolayer on each of the three surfaces. The data shown in these figures for the Pt(111) surface come from our recent experiments reported elsewhere [15].

The addition of Sn in the surface of the alloy decreases the reactivity of the surface and alters the selectivity for the dissociation products. Fig. 14 gives a comparison between the principle products from Pt(111), CO and H_2, on all three surfaces. Addition of Sn eliminates pathways on Pt(111) for complete dehydrogenation of methyl nitrite to form CO, H_2, and surface carbon. In the top panel, all of the CO signal below 400 K for all three surfaces is due to cracking fractions of other products. The small CO peaks at 420–430 K on the alloys can be attributed to CO contamination on the surface prior to dosing methyl nitrite. As shown in the bottom panel, there is no H_2 desorption from either alloy surface. In addition to these TPD results, AES measurement of the alloy surfaces after TPD experiments showed that no carbo-

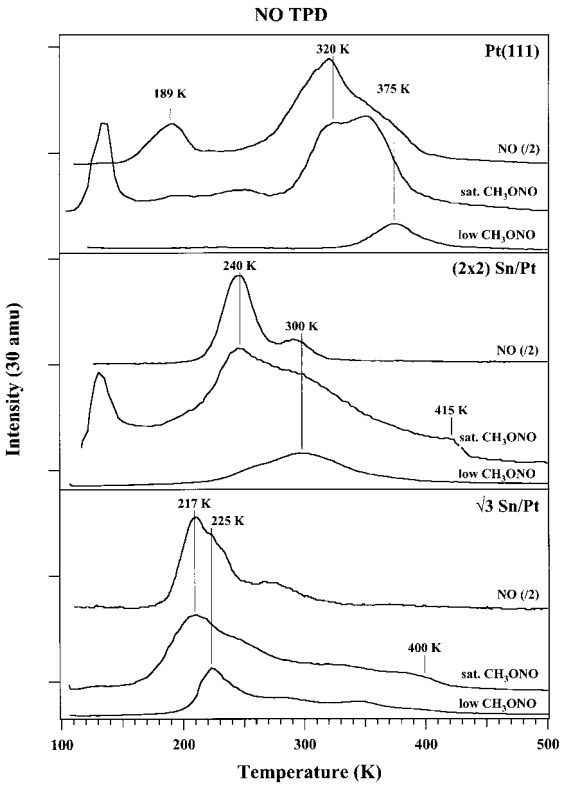

Fig. 15. TPD spectra at 30 amu from Pt(111) and the (2×2) and $\sqrt{3}$ Pt–Sn surface alloys after 0.30 L and 0.05 L exposures of CH_3ONO. These spectra can be used to follow desorption of NO. The upper curve shown for each of the three surfaces reproduces NO TPD spectra taken after NO saturation exposures on the respective surfaces.

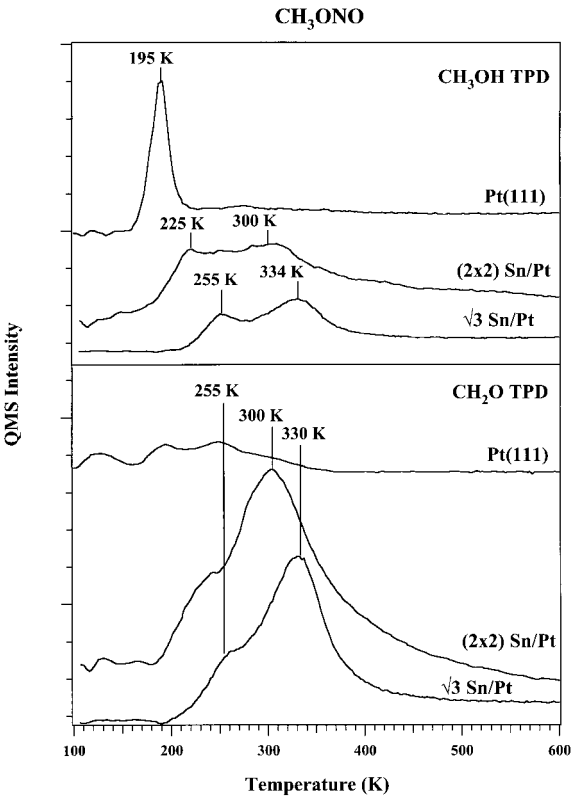

Fig. 16. TPD spectra at 32 and 29 amu following 0.30 L CH_3ONO exposures on Pt(111) and the (2×2) and $\sqrt{3}$ Pt–Sn surfaces. These spectra can be used to follow desorption of methanol (CH_3OH) and formaldehyde ($H_2C{=}O$).

naceous residue was produced, in contrast to that on Pt(111) [15].

Cleavage of the O–NO bond is still facile on the alloys, but the extent of dissociation of the monolayer decreases with increasing Sn concentration. Fig. 15 compares three NO TPD curves for each of the three surfaces: NO desorption after adsorption of a monolayer of NO [33] and NO desorption from monolayer and submonolayer coverages of methyl nitrite. NO adsorption on Pt(111) leads to a well-known coverage of $H_{NO}=0.5$ ML [33], and comparison of the NO desorption peak areas for NO adsorption and CH_3ONO decomposition on the Pt(111) surface directly provides the saturation coverage of methyl nitrite of $H_{CH_3ONO}=0.24$ ML on the Pt(111) surface since methyl nitrite is completely irreversibly adsorbed. Similarly, on the alloys, the amount of methyl nitrite dissociation can be calculated, and this decreases from 0.17 ML on the (2×2) alloy to 0.14 ML on the $\sqrt{3}$ alloy. Uptake curves indicate that the saturation monolayer coverage of methyl nitrite on the three surfaces is the same, and so the extent of dissociation of the methyl nitrite monolayer decreases from 100% on the Pt(111) surface to 70% on the (2×2) and 58% on the $\sqrt{3}$ surface. NO evolution from methyl nitrite decomposition is always desorption rate-limited on all three surfaces, and so coadsorption and site-blocking effects of NO play a role in the observed chemistry. We feel that the high-temperature ''tail'' to the NO evolution from methyl nitrite decomposition at high coverages on the alloys is not due to NO desorption, but some-

how arises as a consequence of the high-temperature evolution of methanol and formaldehyde.

The major hydrocarbon desorption products on the Pt–Sn surface alloys are methanol and formaldehyde, and Fig. 16 compares TPD spectra for CH_3OH and $H_2C{=}O$ on the three surfaces. Methanol TPD spectra show several interesting trends. First, alloying causes an increase in the yield of methanol, and secondly, the methanol product is desorbed at much higher temperatures on the alloys. Methanol desorbs from Pt(111) in a desorption rate limited peak at 195 K, but desorbs in reaction rate-limited peaks at 225 and 300 K on the (2×2) alloy, and 255 and 334 K on the $\sqrt{3}$ alloy. On each of the alloys, the low and high-temperature peaks arise from different rate limiting steps, where hydrogenation of methoxy is affected by the availability of surface hydrogen. We believe that the peak at low temperatures (225 K) arises from facile hydrogenation of methoxy using hydrogen from low-temperature production of formaldehyde, and then another peak appears at higher temperatures (300–340 K), coincident with the desorption of formaldehyde, which frees up sites for further methoxy decomposition and liberation of hydrogen.

The other hydrocarbon product observed in TPD from these alloy surfaces is formaldehyde, which desorbs primarily at 300 and 334 K on the (2×2) and $\sqrt{3}$ alloys, respectively, as shown in Fig. 16. Much of the formaldehyde produced from methoxy decomposition on the alloy surfaces desorbs at higher temperatures than was previously observed (240 K) for formaldehyde desorption after formaldehyde adsorption on Pt(111) [32]. Because we expect that formaldehyde adsorption would be weaker on the alloys, the desorption kinetics of the formaldehyde product are reaction rate-limited by the dissociation of methoxy, and so the formaldehyde desorption activation energy sets a lower limit on the activation energy for dehydrogenation of methoxy to be about 15–16 kcal mol^{-1} on the alloy surfaces. The smaller evolution of formaldehyde at 240 K could be from a desorption rate limited process. No CO or H_2 desorption was observed, indicating that formaldehyde is reversibly adsorbed on the alloys and that the barrier to formaldehyde dehydrogenation on the alloys exceeds 15–16 kcal mol^{-1}. The reaction of methyl nitrite on the alloy surfaces is clean, and no carbon is present on the surfaces after TPD. The selectivity of the Pt(111) surface for producing formaldehyde is increased by the addition of Sn. The alloy surfaces produce a tenfold greater concentration of formaldehyde in TPD compared to the Pt(111) surface.

While further spectroscopic studies are necessary to probe this interesting chemistry, by using these TPD results we can propose a tentative model for the reaction of methyl nitrite on the Pt–Sn surface alloys. Essentially the same mechanism is operative on both surfaces, with only small changes in the adsorption/desorption energies and activation energies on the two surfaces. The desorption of NO in TPD at 240 and 217 K from the (2×2) and $\sqrt{3}$ alloy surfaces, respectively, places an upper limit of 11–13 kcal mol^{-1} on the dissociation energy of the O–NO bond of methyl nitrite. After the dissociation of some of the methyl nitrite, the surface is covered with NO, methoxy species, and unreacted methyl nitrite. Molecular desorption of methyl nitrite and the initial desorption of methanol both occur at $\approx$250 K on the alloys, indicating that the low-temperature, reaction-rate-limited methanol evolution from hydrogenation of methoxy is dependent on hydrogen evolved from methoxy decomposition at sites made available by the desorption of unreacted methyl nitrite and/or coadsorbed NO. After all the molecular methyl nitrite desorbs, we imagine that the surface contains only adsorbed methoxy. Above 300 and 330 K on the (2×2) and $\sqrt{3}$ Pt–Sn alloys, respectively, methoxy decomposes and large simultaneous TPD peaks occur for formaldehyde and methanol at these temperatures.

The reaction rate limited formaldehyde evolution sets an upper limit for the activation energy for dissociation of surface methoxy on the Pt–Sn alloys of 15–16 kcal mol^{-1} on the alloy surfaces. The coincidence of the formaldehyde and methanol TPD peaks indicates that hydrogenation of methoxy to form methanol occurs quite efficiently from the hydrogen produced in the dehydrogenation of methoxy. The formaldehyde produced in

this dehydrogenation reaction is reversibly adsorbed on the alloy surfaces, i.e. it undergoes no further decomposition and desorbs molecularly in TPD.

These results also indicate that we can tune the methyl nitrite–surface interactions by alloying Pt with Sn, and we see some influence of varying the concentration of Sn in the alloy. The formation of CO and H_2 is eliminated on the (2×2) alloy, enhancing desorption of a formaldehyde product by a factor of 10 and a methanol product by a factor of three compared to Pt(111). On the $\sqrt{3}$ alloy, the surface reactivity is reduced further, increasing the amount of methyl nitrite that is reversibly adsorbed and decreasing the yields of formaldehyde and methanol. The relative amounts of formaldehyde and methanol produced during TPD are about the same on the two alloys.

The observation of a gas phase formaldehyde product from methyl nitrite decomposition is not unique to the Pt–Sn surface alloys. Pressley et al. [14] used EID to induce O–N bond cleavage in methyl nitrite adsorbed on the Ag(111) surface ultimately to form a minor gas phase formaldehyde product. Gas phase formaldehyde was also produced from the dissociation of methanol on Cu and Ag surfaces [41–43]. In all of these experiments, formaldehyde desorbs at temperatures of $\approx$250 K. We believe that the high-temperature formaldehyde desorption observed on the Pt–Sn surface alloys in this study is the result of the stabilization of the methoxy intermediate on the alloys because of an increased activation barrier for the cleavage of the C–H bonds.

Suprisingly, not much information is available about the chemistry of methoxy on Pt(111). While methanol decomposition was the subject of numerous studies on Pt(111) and oxygen-precovered Pt(111) [41–58], more recent experiments indicate that the dissociation of methanol on Pt(111) was an artifact induced by defect sites [22,57]. On these defect sites, Secondary Ion Mass Spectrometry (SIMS) studies have shown that the decomposition of methanol proceeds through a methoxy intermediate [54]. Sexton [43], using HREELS, and Akhter and Henderson [54], using SIMS, showed that decomposition of methoxy occurred at $\approx$140 K on clean, defective Pt(111) to form CO and H_2 as the main products. HREELS work by Franaszczuk et al. [58] after methanol adsorption on the (2×1)Pt(110) surface showed signs of a transient formaldehyde species on the surface after annealing slightly above 200 K. Thus, the methoxy intermediate proposed on this surface also dissociated well below room temperature to ultimately form desorption rate-limited CO and H_2 gas-phase products.

Preadsorbed oxygen on the Pt(111) surface causes an increased temperature for cleavage of the O–H bond in methanol and increased stability of the methoxy intermediate on the surface [43,54]. The dissociation temperature of methoxy increased to 170 K in Sexton's [43] study of oxygen precovered Pt(111). Sexton [43] proposed that transition metal surfaces with low heats of adsorption for CO and H_2 such as Ag and Cu will preferentially form formaldehyde and methanol from adsorbed methoxy intermediates, whereas surfaces with high CO heats of adsorption, such as W, Ru, Pd, Pt and Ni, universally decompose surface methoxy to form gas-phase CO and H_2 [59–63].

Within the context of this model, one would expect that the Pt–Sn alloys would be less reactive for methoxy decomposition than Pt(111) based on experiments on CO adsorption on Pt(111) and the Pt–Sn alloy surfaces. Alloying Sn decreases the CO desorption temperature from 375 K on Pt(111) to 353 and 339 K on the (2×2) and $\sqrt{3}$ alloys, and this corresponds to a reduction in the adsorption energy of CO from 29 to 25 to 24 kcal mol^{-1} as the concentration of Sn was increased from the clean Pt(111) to the $\sqrt{3}$ alloy surface [64]. These alloy surfaces are also less reactive for dissociative H_2 adsorption, indicating a weaker Pt–H bond [64]. Reducing the exothermicity of the methoxy decomposition reaction by decreasing the adsorption energy of the products with the addition of Sn stabilizes the methoxy formed from the dissociation of methyl nitrite to much higher temperatures of 300–340 K. Deactivation of the surface for formaldehyde dehydrogenation leads to elimination of the CO product and the formation of methanol and formaldehyde on the alloy surfaces. The large stabilization of

methoxy on these alloys, from <165 K on Pt(111) [15] to 300–340 K on the two Pt–Sn alloys, is larger than one might expect based on the rather small changes in the CO adsorption energies cited above. This indicates that other factors are important, such as the numbers and distributions of reactive Pt atoms, i.e. ensemble size and site requirements, for methoxy decomposition and changes in the electronic structure of the surface due to alloying.

The analysis of our results leads to the conclusion that the two Pt–Sn alloy surfaces contain high concentrations of surface methoxy, and this is of importance because the adsorption of small alcohols on Pt–Sn alloy surfaces under UHV conditions is reversible, and no alkoxy intermediate is formed [22]. Thus, methyl nitrite can be used as an adsorbed precursor for generating the methoxy intermediate on well-characterized single crystal surfaces in UHV [65]. This is a novel approach that we expect to be important for elucidating the role of methoxy intermediates in surface reactions. As one example, in direct oxidation methanol fuel cells [66–74], electrode poisoning by adsorbates such as H, CHO or CO has been cited as a limiting factor [75]. Researchers seeking to improve this technology have investigated Pt–Ru [76] and Pt–Sn [77–82] electrodes, and new opportunities for preparing organic intermediates on well-defined bimetallic Pt surfaces may be helpful in providing a fundamental understanding of these systems.

5. Conclusions

Nitromethane is only weakly adsorbed (10–10.8 kcal mol^{-1}) on the Sn/Pt(111) surface alloys and shows no thermal reaction, undergoing completely reversible adsorption in TPD. In contrast, methyl nitrite is a much more reactive molecule. Incorporation of Sn into the Pt(111) surface forms Pt–Sn alloys that are less reactive than Pt(111), and this has three major effects on the chemistry of adsorbed methyl nitrite. First, this results in the molecular desorption of 25–40% of the adsorbed methyl nitrite monolayer on the alloy surfaces. The two methyl nitrite desorption peaks in TPD at 225 and 267 K on the (2×2) surface and at 195 and 255 K on the $\sqrt{3}$ alloy surface can be used to estimate adsorption energies of 16.3 and 15.5 kcal mol^{-1}, respectively, for the most strongly bound species. Secondly, alloying Sn into the Pt(111) surface also stabilizes the surface methoxy intermediate produced from the dissociation of the O–NO bond of methyl nitrite to much higher temperatures (300–340 K). This leads to high-temperature, reaction-rate-limited desorption of methanol and formaldehyde products on the alloys. Finally, alloying eliminates the CO and H_2 products from complete decomposition of methyl nitrite on Pt(111) due to a decrease in the dehydrogenation activity for formaldehyde. The selectivity of the Pt(111) surface for desorbing formaldehyde is greatly enhanced with the addition of Sn. These alloy surfaces also show no deposition of surface carbon in post-TPD AES scans; dissociation of methyl nitrite on the Pt–Sn alloys methanol and formaldehyde during TPD. Importantly, we have shown that methyl nitrite can be used as an adsorbed precursor to yield surface methoxy species at low temperatures in significant quantities.

Acknowledgements

This work was partially supported by the Department of Energy, Office of Basic Energy Sciences, Chemical Division and the Army Research Office. The authors would like to thank J. Wang for synthesizing the methyl nitrite sample and J.M. White for making his results available to us prior to their publication. J.W.P. gratefully thanks the Department of Education for a graduate research fellowship.

References

[1] K.I. Zamaraev, M.I. Khramov, V.N. Parmon, Cat. Rev. Sci. Eng. 36 (1994) 617.
[2] J.B. Benziger, Combust. Sci. Tech. 29 (1982) 195.
[3] C.P. Sutton, Rocket Propulsion Elements, Wiley, New York, 1963.
[4] K.R. Brower, J. Org. Chem. 53 (1988) 3776.
[5] J.B. Benziger, Appl. Surf. Sci. 17 (1984) 309.
[6] S.Y. Hwang, A.C.F. Kong, L.D. Schmidt, Surf. Sci. 217 (1989) 179.

[7] N. Saliba, J. Wang, B.A. Bansenaur, B.E. Koel, Surf. Sci. 389 (1997) 147.
[8] J. Wang, N. Saliba, B.A. Banasaur, B.E. Koel, Langmuir, in press.
[9] Q. Chen, S. Haq, B.G. Frederick, N.V. Richardson, Surf. Sci. 368 (1996) 310.
[10] S.C. Chang, C. Wang, L.J. Fan, Y.C. Tang, A. Hamelin, J. Electroanal. Chem. 415 (1996) 169.
[11] O. Semin, J. Wang, B.E. Koel, to be published.
[12] A.M. Wodtke, E.J. Hintsa, Y.T. Lee, J. Chem. Phys. 84 (1986) 1044.
[13] M.J. Dewat, J.R. Ritchie, J. Alster, J. Am. Chem. Soc. 50 (1985) 1031.
[14] L.A. Pressley, E.D. Pylant, J.M. White, Surf. Sci. 367 (1997) 1.
[15] J.W. Peck, D. Mahon, D. Beck, B.A. Bansenaur, B.E. Koel, to be published.
[16] M.T. Paffett, S.C. Gebhard, R.G. Windham, B.E. Koel, Surf. Sci. 223 (1989) 449.
[17] C. Xu, B.E. Koel, Surf. Sci. 304 (1994) 249.
[18] C. Xu, B.E. Koel, M.T. Paffett, Langmuir 10 (1994) 166.
[19] Y.-L. Tsai, B.E. Koel, J. Phys. Chem. 101 (1997) 2895.
[20] C. Xu, Y.-L. Tsai, B.E. Koel, J. Phys. Chem. 98 (1994) 585.
[21] C. Xu, B.E. Koel, M.A. Newton, N.A. Frei, C.T. Campbell, J. Phys. Chem. 99 (1995) 16670.
[22] C. Panja, N. Saliba, B.E. Koel, Surf. Sci. 395 (1998) 248.
[23] C. Xu, Y.-L. Tsai, B.E. Koel, J. Phys. Chem. 98 (1994) 585.
[24] C. Xu, B.E. Koel, Surf. Sci. 292 (1993) L803.
[25] M.T. Paffett, S.C. Gebhard, R.G. Windham, B.E. Koel, Surf. Sci. 2 (1989) 449.
[26] S.H. Overbury, D.R. Mullins, M.T. Paffet, B.E. Koel, Surf. Sci. 254 (1991) 45.
[27] A. Atrei, U. Bardi, J.X. Wu, E. Zanazzi, G. Rovida, Surf. Sci. 290 (1993) 286.
[28] M. Galeotti, A. Atrei, U. Bardi, G. Rovida, M. Torrini, Surf. Sci. 313 (1994) 349.
[29] F.L. Rook, J. Chem. Eng. Data 27 (1982) 72.
[30] P.N. Ghosh, Hs.H. Gunthard, Spect. Acta 37A (1981) 347.
[31] M.P. Irion, A. Selinger, A.W. Castleman, Jr, E.E. Ferguson, K.G. Weil, Chem. Phys. Lett. 147 (1988) 33.
[32] M.A. Henderson, G.E. Mitchell, J.M. White, Surf. Sci. 188 (1987) 206.
[33] C. Xu, B.E. Koel, Surf. Sci. 310 (1994) 198.
[34] P.A. Redhead, Vacuum 12 (1962) 203.
[35] C. Xu, B.E. Koel, Surf. Sci. 304 (1994) L505.
[36] N. Saliba, C. Panja, B.E. Koel, to be published.
[37] J. Segner, W. Vielhaber, G. Ertl, Israel J. Chem. 22 (1982) 375.
[38] D. Dahlgren, J.C. Hemminger, Surf. Sci. 123 (1982) L739.
[39] M.E. Bartram, R.G. Windham, B.E. Koel, Surf. Sci. 184 (1987) 57.
[40] M. Voss, H. Busse, B.E. Koel, to be published.
[41] I.E. Wachs, R.J. Madix, Surf. Sci. 76 (1978) 531.
[42] I.E. Wachs, R.J. Madix, J. Catal. 53 (1978) 208.
[43] B.A. Sexton, Surf. Sci. 88 (1979) 299.
[44] M. Bowker, R.J. Madix, Surf. Sci. 95 (1980) 190.
[45] D.W. Goodman, J.T. Yates, T.E. Madey, Surf. Sci. 93 (1980) L135.
[46] J.B. Benziger, R.J. Madix, J. Catal. 65 (1980) 36.
[47] E.I. Ko, J.B. Benziger, R.J. Madix, J. Catal. 62 (1980) 264.
[48] D.M. Hanson, R. Stockbauer, T.E. Madey, J. Chem. Phys. 77 (1982) 1569.
[49] E.I. Ko, R.J. Madix, Surf. Sci. 112 (1981) 373.
[50] S.L. Miles, S.L. Bernasek, J. Phys. Chem. 87 (1983) 1626.
[51] P.H. McBreen, W. Erley, H. Ibach, Surf. Sci. 133 (1983) L469.
[52] J.A. Gates, L.L. Kesmodel, J. Catal. 83 (1983) 437.
[53] I.F. Tindall, J.C. Vickerman, Surf. Sci. 149 (1985) 577.
[54] S. Akhter, J.M. White, Surf. Sci. 167 (1986) 101.
[55] J.L. Davis, M.A. Barteau, Surf. Sci. 187 (1987) 387.
[56] J. Wang, R.I. Masel, Surf. Sci. 243 (1991) 199.
[57] K.D. Gibson, L.H. Dubois, Surf. Sci. 223 (1990) 59.
[58] K. Franaszczuk, E. Herrero, P. Zelenay, A. Wieckowski, J. Wang, R.I. Masel, J. Phys. Chem. 96 (1992) 8509.
[59] H. Luth, G.W. Rubloff, W.D. Grobman, Surf. Sci. 63 (1977) 325.
[60] H.J. Krebs, H. Luth, in: Vibrations in Adsorbed Layers, Proc. Jülich Conf., 1978.
[61] G.W. Rubloff, J.E. Demuth, J. Vacuum Sci. Tech. 14 (1977) 419.
[62] G.B. Fisher, T.E. Madey, B.J. Waclwaski, J.T. Yates, in: Proc. 7th Int. Vacuum Congr. 3rd Int. Conf. Solid Surfaces, Vienna, Vol. II, 1977, p. 1071.
[63] W.F. Egelhoff, J.W. Linnett, D.L. Perry, Faraday Disc. Chem. Soc. 60 (1975) 127.
[64] M.T. Paffet, S.C. Gebhard, R.G. Windham, B.E. Koel, J. Phys. Chem. 94 (1990) 6831.
[65] J.W. Peck, D. Mahon, D. Beck, B.E. Koel, J. Phys. Chem. submitted.
[66] S. Surampudi, S.R. Narayanan, E. Vamos, H. Frank, G. Halpert, A. La Conti, J. Kosek, G.K. Surya Prakash, G.A. Olah, J. Power Sources 47 (1994) 377.
[67] C. Lamy, Electrochim. Acta 29 (1984) 1581.
[68] K. Ota, Y. Nakagawa, M. Takahashi, J. Electroanal. Chem. 179 (1984) 179.
[69] E.M. Belgsir, H. Huser, J.M. Leger, C. Lamy, J. Electroanal. Chem. 225 (1987) 281.
[70] F. Kadigam, B. Beden, J.M. Leger, C. Lamy, J. Electroanal. Chem. 129 (1981) 89.
[71] M. Shibata, S. Motoo, J. Electroanal. Chem. 229 (1987) 385.
[72] K. Kunimatsu, J. Electroanal. Chem. 213 (1986) 149.
[73] P. Olivi, B. Beden, F. Hahn, J.M. Leger, C. Lamy, J. Electroanal. Chem. 346 (1993) 415.
[74] B. Beden, S. Juanto, J.M. Leger, C. Lamy, J. Electroanal. Chem. 238 (1987) 323.
[75] R. Parsons, T. Vandernoot, J. Electroanal. Chem. 257 (1988) 9.
[76] M.M.P. Janssen, J. Moolhuysen, Electrochim. Acta 21 (1976) 869.
[77] M.M.P. Janssen, J. Moolhuysen, Electrochim. Acta 21 (1976) 861.
[78] M.M.P. Janssen, J. Moolhuysen, J. Catal. 46 (1977) 289.
[79] K.J. Cathro, J. Electrochem. Soc. 116 (1969) 1608.
[80] S. Szabo, J. Electroanal. Chem. 172 (1984) 359.
[81] S. Gilman, M.W. Breiter, J. Electrochem. Soc. 109 (1962) 1099.
[82] A. Haner, N.R. Philip, J. Phys. Chem. 95 (1991) 3740.